Heliyon 10 (2024) e39614

Contents lists available at ScienceDirect

Heliyon

journal homepage: www.cell.com/heliyon

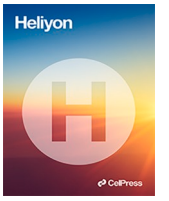

Research article

Improving mortar properties using traditional ceramic materials ground to precisely controlled sizes

Luciane Farias Ribas [a], Guilherme Chagas Cordeiro [b], Romildo Dias Toledo Filho [c], Moises Frías [d], Luis Marcelo Tavares [e,*]

[a] Department of Civil Engineering, Universidade do Estado do Amazonas – UEA, Manaus, AM, Brazil
[b] Laboratory of Civil Engineering, Universidade Estadual do Norte Fluminense Darcy Ribeiro – UENF, Campos dos Goytacazes, RJ, Brazil
[c] Department of Civil Engineering, Universidade Federal do Rio de Janeiro – COPPE/UFRJ, Rio de Janeiro, RJ, Brazil
[d] Eduardo Torroja Institute for Construction Science – IETcc-CSIC, Madrid, Spain
[e] Department of Metallurgical and Materials Engineering, Universidade Federal do Rio de Janeiro – COPPE/UFRJ, Rio de Janeiro, RJ, Brazil

ARTICLE INFO

Keywords:
Construction and demolition waste
High-energy grinding
Pozzolanic activity
Packing density
Pore size distribution

ABSTRACT

The present work investigates the impact of particle size reduction of traditional ceramic materials as partial substitutes for Portland cement in mortars. Ceramic brick, ceramic tile, and stoneware were selected, with three particle sizes (D_{50} of 1, 5, and 15 μm) achieved through grinding operations adapted to each material grindability. The reactivity of ceramic powders was assessed via dissolution in saturated lime solution. Mortars were prepared with 10 % and 20 % cement mass replaced by ceramic powders ground to each fineness. The packing density of mortars was evaluated using the Compressible Packing Model. Compressive strength was measured at 1, 3, 7, and 28 days, and pore size distribution was analyzed by mercury intrusion porosimetry. Results indicated that ceramic tile required less grinding energy than brick and stoneware. High-energy grinding slightly altered the crystalline structure and increased amorphous content, enhancing reactivity with lime. Increased cement replacement with finer ceramic powders (D_{50} about 1 μm) improved strength, increased mesopores (50 nm), and reduced pore size threshold, attributed to filler and pozzolanic effects. A multiple linear regression model effectively described the influence of various variables on mortar strength with the interaction terms demonstrating the complexity of the interplay of the variables.

1. Introduction

Construction and demolition waste (CDW) is defined as a material generated during the construction, renovation, demolition, or dismantling of structures such as buildings, roads, and bridges. Construction waste originates from construction and renovation activities, including leftover materials such as concrete, bricks, wood, plaster, metals, and various used in packaging. In contrast, demolition waste consists of materials resulting from the destruction of pre-existing structures, encompassing debris from concrete, masonry, metals, and wood, often mixed with materials such as glass and plastics. Globally, CDW represent approximately 30 % of total solid waste generated [1], which can be reused and recycled in various applications, contributing to sustainability and the circular

* Corresponding author. Department of Metallurgical and Materials Engineering, Universidade Federal do Rio Janeiro, Center of Technology, I-216, Rio de Janeiro, Brazil.
E-mail address: tavares@ufrj.br (L.M. Tavares).

https://doi.org/10.1016/j.heliyon.2024.e39614
Received 30 June 2024; Received in revised form 17 October 2024; Accepted 18 October 2024
Available online 19 October 2024

economy in the construction sector. Among CDW, brick waste is a significant component of construction and demolition activities worldwide [2].

One of the primary applications of CDW is as coarse and fine aggregates for the production of concrete and mortar, partially or completely replacing natural materials [3,4]. Additionally, CDW can be utilized in paving projects as base and sub-base layers for roads, providing both economic and environmentally beneficial solutions [5]. Other applications include its use in sanitary landfills as cover material, with significant landslide risks [6], in the manufacture of eco-friendly blocks and bricks [7], in the soil improvement [8], and in the recovery of degraded areas [9]. The recycling of gypsum waste for the production of new gypsum products and the recovery of metals for smelting and manufacturing new metallic components are also effective ways to reuse CDW [10,11]. These practices not only reduce the need for natural resource extraction but also minimize the environmental impacts associated with improper waste disposal.

The use of CDW as aggregates for concrete presents several advantages and disadvantages that must be carefully considered. Among the advantages are the reduction in natural resource extraction and the decrease in the volume of waste sent to landfills, thereby reducing the environmental impact of improper disposal [12]. However, the use of CDW as aggregates for concrete also has some drawbacks. The high cost of recycling is one of the main disadvantages, which can be mitigated by the inclusion of landfill and incineration taxes [13]. The quality and uniformity of recycled aggregates can vary significantly, potentially affecting the mechanical properties and durability of the concrete. The presence of fine and ultrafine particles in recycled aggregates can be particularly problematic. These fines can increase the water demand of the concrete, negatively influencing its workability, water absorption, and mechanical strength [3].

To mitigate these challenges, the fine fraction of CDW can be processed and used as a supplementary cementitious material (SCM) [14]. This SCM can be incorporated into concrete as partial substitutes for Portland cement, contributing to the improvement of certain properties of concrete, such as compressive strength and durability [15]. This material can exhibit latent hydraulic behavior (occasionally erroneously referred to as pozzolanic effects) when predominantly composed of concrete and mortar waste [15,16]. Li et al. [17] demonstrated that recycled concrete powder can improve the flowability and early strength of cement pastes, especially at replacement levels up to 30 %. With 10 % recycled concrete powder, the hydration induction period of a cement-based paste was extended, while both the peak exothermic rate and total heat release decreased. On the other hand, studies have shown that the addition of recycled concrete powder significantly reduced the induction period of cement pastes and substantially increased the hydration heat, especially when the waste material is ultrafine [18].

In addition to the hydration/rehydration of cement-based phases, CDW fines can exhibit pozzolanic behavior when composed of ceramic waste, such as tiles, bricks, stoneware, and sanitary ware [2,19]. Specifically, Reig et al. [20] highlighted that a significant amount of ceramic waste is generated annually as part of CDW or from losses in factories. These materials can exhibit amorphous or disordered lattice structures from the dehydroxylation of clay minerals during the ceramic production processes. The presence of these silica- and alumina-rich phases explains the potential pozzolanic character of these wastes. Recycled clay brick powder was utilized as a partial cement replacement in cement-based pastes and mortars, resulting in an increase in compressive strength with replacement levels of up to 20 % [21]. Additionally, the hydration products included C-S-H, C-A-H, and C-A-S-H, with the pozzolanic reaction of recycled clay brick powder mainly occurring between 60 and 90 days. Hoppe Filho et al. [22] observed that the partial replacement of cement with recycled ceramic waste altered the microstructure of the hydrated paste by increasing the ettringite content and promoting the formation of monocarboaluminate. In this case, the highest portlandite consumption was observed between 7 and 28 days, coinciding with increased monocarboaluminate formation.

Linked with the chemical potential of the fine and ultrafine fractions of CDW, significant physical effects can be achieved by partially replacing cement with this waste. Grinding-induced particle size reduction has been identified as the driving factor behind increased heterogeneous nucleation, fostering the creation of new nucleation sites for hydrated product deposition [23]. Zhao et al. [24] observed that reducing the particle size of recycled clay brick powder enhances its performance. They noted that finer recycled powder particles contribute more to compressive strength due to their increased specific surface area and lower surface binding energy. Li et al. [25] found that reduction in particle size of recycled clay brick powder improved the compressive strength of blended mortar due to decreased porosity and increased pore tortuosity. De Matos et al. [26] investigated the effect of ceramic tile demolition waste as cement replacement on the early-age performance of pastes and observed a reduction of the interparticle distance in the system due to the higher specific surface area of the waste and increased volumetric particle concentration. Ultrafine ceramic powder with a mean particle size of 3.5 μm, ground from ceramic waste, was used to partially replace cement in mortars [27]. The results showed that this ceramic powder refined the mortar pore structure due to its physical filling and pozzolanic effects.

In this scenario, the current study investigates the impact of particle size reduction by grinding of different ceramic materials to precisely controlled sizes, assessing their feasibility as partial replacements for Portland cement in mortars. Bricks, roof tiles, and stoneware, representing potential wastes from the ceramic component of CDW, were employed for this purpose. The novelty of this study lies in evaluating these three distinct ceramic materials with significantly different and highly controlled particle sizes to understand their impact on mortar properties. The utilization of the ceramic fraction of CDW as SCM can be particularly attractive given the stagnation of traditional SCM sources, such as fly ash and blast-furnace slag [28,29]. The decline in availability of these conventional materials is driven by factors such as the reduction in coal-fired power generation and shifts in industrial processes. Consequently, exploring alternative sources like ceramic waste not only addresses the supply gap but also promotes sustainable waste management practices.

Table 1
Chemical composition (% in mass) of Portland cement (PC) and ceramic samples.

Oxide (wt.%)	PC	BC15	BC5	BC1	TC15	TC5	TC1	SW15	SW5	SW1
SiO_2	20.9	57.0	58.6	51.2	53.1	56.9	47.6	68.7	69.0	51.5
Al_2O_3	5.2	31.8	29.2	22.1	33.1	30.1	23.0	16.7	16.5	11.7
K_2O	0.3	1.0	1.0	1.0	2.5	2.5	2.6	2.8	2.6	2.6
CaO	64.3	0.2	0.2	0.1	0.2	0.2	0.2	1.0	0.9	1.0
MgO	1.3	0.4	0.4	0.3	0.8	0.7	0.5	1.3	1.3	0.9
Fe_2O_3	4.15	6.8	7.3	17.9	6.4	5.6	16.7	6.5	6.4	24.9
SO_3	2.81	0.0	0.0	0.1	0.0	0.0	0.0	0.0	0.1	0.1
TiO_2	–	0.8	0.9	0.8	1.4	1.0	1.4	0.7	0.6	0.6
Na_2O	0.1	0.1	0.1	0.6	0.3	0.4	0.7	1.3	1.4	1.3
Cr_2O_3	–	0.0	0.2	2.6	0.0	0.2	2.5	0.0	0.2	3.7
Free CaO	2.4	–	–	–	–	–	–	–	–	–
Other oxides	–	0.2	0.2	1.1	0.3	0.3	1.3	0.4	0.4	1.7
Loss on ignition	1.6	1.8	1.9	0.9	1.9	2.1	2.1	0.6	0.6	0.0

2. Experimental

2.1. Materials

Ceramic brick (BC), red tile (TC), and stoneware (SW), acquired from the local commerce at Rio de Janeiro (Brazil), were used as the basis for this investigation. Mortars were formulated using Brazilian standard sand [30], ordinary Portland cement (density of 3140 kg/m^3 and Blaine fineness of 375 m^2/kg), and ether carboxylic-based superplasticizer (density of 1077 kg/m^3 and 31 % oven-dried residue). The chemical composition of Portland cement (named PC) is summarized in Table 1.

2.2. Methods

Laboratory jaw and cone crushers were employed for the initial crushing of the ceramic materials. Subsequently, all materials underwent dry grinding in a closed-circuit ball mill (30.6 cm in diameter and 31.7 cm in length), as detailed elsewhere [31]. Grinding media consisted of steel balls (16-mm diameter), and grinding was carried out to ensure that particle size distributions comparable to those of Portland cement were reached, namely with a median particle size (D_{50}) of 15 μm. Following this initial grinding stage, the product underwent wet grinding using a high-energy mill (1-S attritor mill from Union Process, Inc.). Initially, samples were ground in batch mode to generate a product with D_{50} of approximately 5 μm, employing 6-mm steel balls and grinding at 150 rpm. Grinding times were varied around 1 h, taking into account the different grindabilities of the samples, as discussed in Section 3.1.

A final wet grinding step in the same batch mill involved the product from the former stage, with the use of 3-mm steel balls. Dispersion during grinding was facilitated by addition of a 1 % solution of sodium hexametaphosphate as grinding aid. This final stage yielded a product with D_{50} of approximately 1 μm, demanding batch grinding times around 8 h, but that varied as a function of grindability of each sample. A total of nine ground samples were prepared, identified as BC, TC, and SW, with representative particle sizes (D_{50}) of approximately 1, 5, and 15 μm, achieved after each grinding stage (e.g., 'BC15' is the ceramic brick with about 15 μm D_{50} size).

To assess the grindability of the ceramic samples, the standard Bond ball mill grindability test [32] was employed, with feed samples with size below 3.35 mm and a closing sieve of 45 μm, resulting in the Bond ball mill work index. Particle size distributions were determined via laser scattering using the Malvern Mastersizer 2000 analyzer. Density measurements were conducted using a Micromeritics AccuPyc II 1340 pycnometer. Oxide composition analyses were performed using an X-ray fluorescence spectrometer (Axios Max Panalytical with a 4 kW Rh tube) and the loss on ignition was obtained according to ABNT NBR NM 18 [33]. The specific surface area of all ceramic powders was assessed by the BET method from adsorption of nitrogen gas using an ASAP 2020 V3.01 analyzer.

X-ray diffraction analyses were conducted using a Bruker-AXS D4 Endeavor instrument operating under the specified conditions: Co Kα (40 kV, 40 mA), with a step size of 0.02°, 1 s counting time per step employing a linear detector sensitive to the position, type silicon drift LynxEye, and scanning from 10 to 60° 2θ angles. Quantitative analysis was performed using the Rietveld refinement method with Bruker-AXS Topas v. 4.2 software. Crystalline structure information for refined phases was obtained from the Bruker-AXS database or the International Crystal Structure Database (ICSD). Amorphous content was quantified using approximately 20 wt% of ultrafine lithium fluoride (LiF) as internal standard. Thermal behavior of samples was investigated using an SQT 600 simultaneous DSC-TGA instrument (TA Instruments) from room temperature up to 1000 °C, employing a heating rate of 10 °C/min under a dynamic N_2 atmosphere (100 cm^3/min).

The reactivity of the ceramic powders was assessed using the dissolution method in lime-saturated solution [34]. This procedure involved immersing 1 g of sample in plastic containers along with 75 ml of lime-saturated solution, prepared by dissolving 2 g of calcium hydroxide in 1 L of distilled water. The sealed containers were then incubated at 40 ± 1 °C for 1, 7, 28, and 90 days. After each aging period, the concentration of CaO in the solution was determined by titration with HCl. The fixed lime concentration (mM/L) was calculated by subtracting the concentration in the lime-saturated solution from the CaO content in the solution in contact with the sample at the conclusion of the specified period.

Table 2
Superplasticizer (SP) content in mortars (% by binder mass).

Mortar	SP content (%)	Mortar	SP content (%)
M-REF	0.02	M20-BC5	0.17
M10-BC15	0.06	M20-TC5	0.17
M10-TC15	0.08	M20-SW5	0.02
M10-SW15	0.06	M10-BC1	0.17
M20-BC15	0.10	M10-TC1	0.19
M20-TC15	0.17	M10-SW1	0.19
M20-SW15	0.07	M20-BC1	0.60
M10-BC5	0.12	M20-TC1	0.60
M10-TC5	0.12	M20-SW1	0.60
M10-SW5	0.02		

Mortars were formulated to assess the performance of ceramic samples in conjunction with cement. In this case, a reference mortar (M-REF) was prepared with water-to-cement and sand-to-cement ratios of 0.48 and 3.0, respectively. A superplasticizer content of 0.02 % was utilized to achieve a 225 mm spreading diameter [35]. Subsequently, mortars were formulated with partial cement replacement of 10 % and 20 % by the ceramic powders ground to different fineness. The mortars were identified according to replacement content and representative ceramic particle size (e.g., M10BC15 representing mortar with 10 % cement replacement by 15-μm ceramic brick). It is worth noting that variable contents of the superplasticizer (0.02–0.60 %) were required in mortars containing ceramic powders to maintain the spread within the range of 210–230 mm, as indicated in Table 2.

Cylindrical mortar specimens with 50 mm in diameter and 100 mm in height were cast and maintained into the molds for 24 h. The specimens were then demolded and immersed in saturated lime water at 21 °C until tests of compressive strength (1, 7, and 28 days) and pore size distribution (28 days). Compressive strength tests were carried out in a universal testing machine Shimadzu AGX 100 kN at a displacement rate of 0.1 mm/min. Pore size distribution was analyzed using a Micromeritics Autopore IV device according to ISO 15901-1 standard [36]. A pressure of 40.000 psi was used and the 140° of contact angle was admitted [37]. The analyzes were conducted on 1 cm^3 cubes extracted from the median portion of the cylindrical specimens.

The results from mortar tests were analyzed statistically by analysis of variance with a significance level (α) of 0.05. Multiple comparisons were made using Tukey's test [38]. In addition, a multiple linear regression model was used to describe the variation of compressive strength as a function of the various variables studied in accordance to **Eq. (1)**.

$$\text{Compressive strength} = \lambda_0 + \sum_{i=1}^{n} \lambda_i x_i + \sum_{i=1}^{n} \lambda_{ii} x_i^2 + \sum_{i=1}^{n} \sum_{j=i+1}^{n} \lambda_{ij} x_i x_j \tag{1}$$

considering λ_0, λ_i and λ_{ij} the various fitted coefficients and x_i the independent variables. In developing the model, the terms were removed one-by-one from the regression, starting with those with the least significant values (highest p-values) using the standard stepwise regression approach [38].

The packing density of all mixes was assessed with the aid of Betonlab Pro3 software, which is based on the Compressible Packing Model (CPM) [39]. CPM allows conversion from a virtual packing density (γ) to the actual packing density ($\varnothing$) of the mix, accounting for the energy applied during the placement process. The virtual packing density of a granular mix with n class of particles can be calculated by **Eq. (2)**:

$$\gamma = \frac{\beta_i}{1 - \sum_{j=1}^{i-1} \left[1 - \beta_i + b_{ij}\beta_i \left(1 - \frac{1}{\beta_j}\right)\right] y_j - \sum_{j=i+1}^{n} \left(1 - a_{ij}\frac{\beta_i}{\beta_j}\right) y_j} \tag{2}$$

considering β_i the virtual packing density of the i^{th} class, y_j the volumetric fraction of class j, and a_{ij} and b_{ij} are interaction coefficients described as loosening and wall effects, respectively, which are calculated using **Eqs. (3)** and **(4)**:

$$a_{ij} = \sqrt{1 - \left(1 - \frac{d_j}{d_i}\right)^{1.02}} \tag{3}$$

$$b_{ij} = 1 - \left(1 - \frac{d_i}{d_j}\right)^{1.5} \tag{4}$$

considering d_i and d_j the diameters of the granular classes i and j, respectively.

The CPM incorporates a scalar parameter, denoted as the compaction index K, which establishes the relationship γ and $\varnothing$ according to **Eq. (5)**:

$$K = \sum_{i=1}^{n} \frac{y_i/\beta_i}{\frac{1}{\varnothing} - \frac{1}{\gamma_i}} \tag{5}$$

Table 3
Physical properties of ceramic samples.

Characteristic	BC15	BC5	BC1	TC15	TC5	TC1	SW15	SW5	SW1
Wi (kWh/t)	16.7	–	–	10.1	–	–	17.6	–	–
D_{50} (μm)	15.0	4.9	1.1	13.6	4.6	1.1	14.8	4.9	1.1
Density (g/cm^3)	2.82	2.78	2.88	2.78	2.72	2.76	2.67	2.66	2.83
BET specific surface area (m^2/kg)	21.45	24.20	36.24	22.90	27.40	45.60	1.46	2.99	23.83

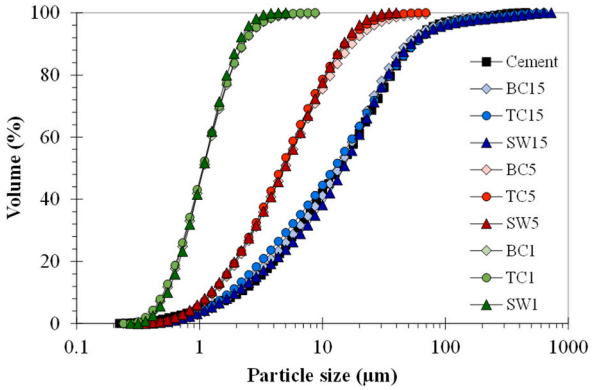

Fig. 1. Particle size distribution of the ground samples and cement.

Table 4
Mineralogical composition of ceramic samples (wt%).

Mineral	BC15	TC15	SW15	BC5	TC5	SW5	BC1	TC1	SW1
Quartz	37	22	41	36	22	41	28	16	32
Intermediate Microcline	9	22	10	8	23	14	8	16	10
Hematite	5	2	4	5	2	4	4	2	3
Muscovite 2M1	7	11	2	6	13	0	5	8	0
Iron α	0	0	1	1	1	2	7	5	8
Amorphous	33	35	33	35	34	29	44	48	41
Others	9	8	9	9	5	10	4	5	6

considering K the compaction index, $\varnothing$ the actual packing density, n the number of particle classes, y_i the volumetric fraction, β_i the virtual packing density of the i^{th} class, and γ_i the virtual packing density when i is the dominant class.

Briefly, CPM enables the calculation of the packing density of a dry granular mix from the knowledge of the particle size distribution of the mix, the virtual packing density of each individual fraction in the mix (β_i), and the compaction index. Subsequently, the packing density of a mortar (or concrete) in the presence of water and superplasticizer can be calculated. In this case, the β_i values for sand are determined as a dry packing density, while those for fine materials are obtained from water demand tests [40]. Therefore, CPM assumes that changes in particle surface forces induced by water and superplasticizer are considered only for fine materials.

According to De Larrard [39], the packing properties of sand and fine materials (cement and ceramic powders) were determined using the vibration and compaction ($K = 9$), and water demand ($K = 6.7$) tests, respectively. For the water demand tests, the superplasticizer dosage was consistent with that used in each mortar (Table 2).

3. Results and discussion

3.1. Characterization of the ceramic powders

The susceptibility of each material to grinding was assessed using the grinding Bond work index (*Wi*), with results summarized in Table 3. Notably, varying energy requirements in grinding were observed across the different materials. Specifically, TC exhibited lower energy demands compared to BC and SW for achieving an equivalent product size. Consequently, size reduction of TC would result in a finer product compared to the other materials [41] if ground under identical conditions. This indicates the distinct breakage rates of the materials [42].

To ensure comparable size distributions among the different materials, grinding parameters were adjusted. Specifically, higher throughput in continuous grinding and shorter grinding durations in batch grinding were employed for TC relative to BC and SW, owing to its comparatively lower *Wi*. Fig. 1 illustrates the particle size distributions of each sample, highlighting the close agreement in

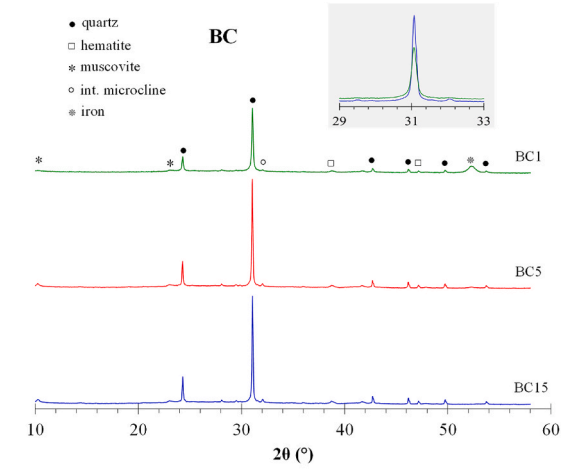

(a)

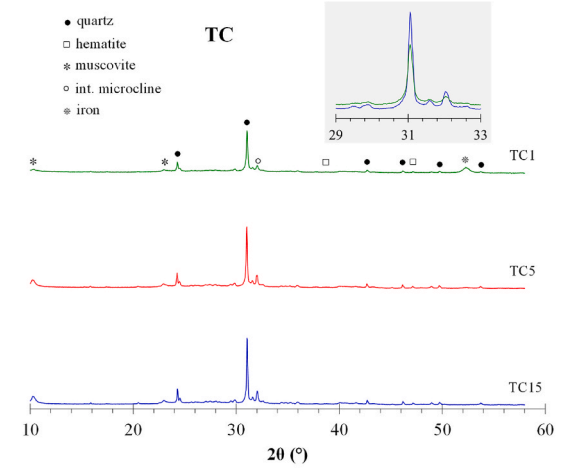

(b)

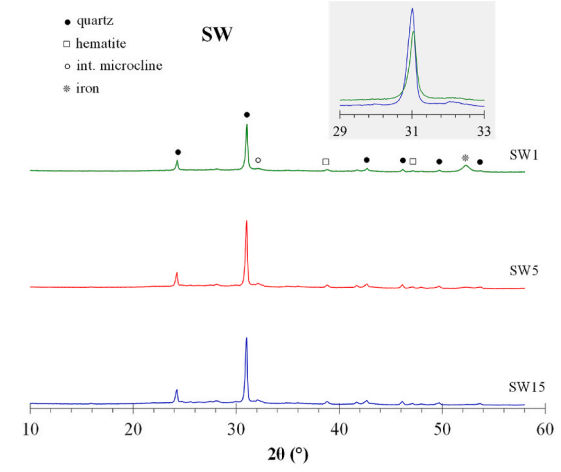

(c)

Fig. 2. XRD patterns of BC (a), TC (b), and SW (c) samples.

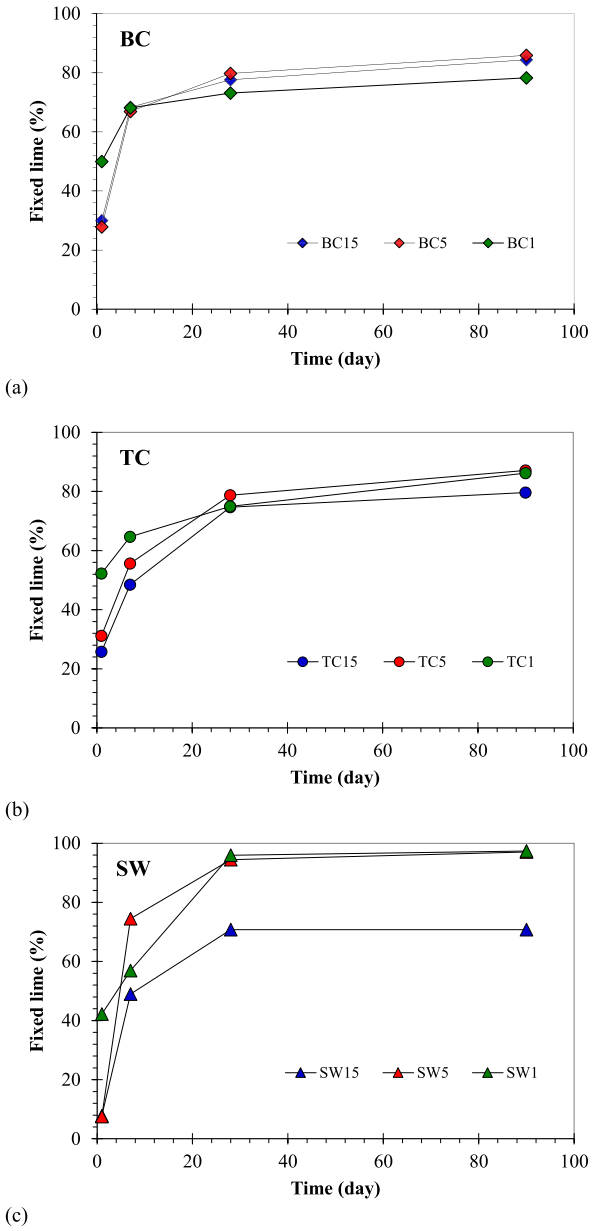

Fig. 3. Variation of fixed lime as a function of time of BC (a), TC (b), and SW (c) samples.

spite of differences in grindability. Such close agreement was particularly critical, since pozzolanic activity is known to be significantly influenced by particle size [43]. As expected, the BET specific surface area increased with the reduction of particle size for the three types of ceramic materials as shown in Table 3. In this instance, it is important to highlight the significant increases in specific surface area observed in the transition of particle sizes from 5 to 1 μm.

Chemical analyses of the materials after each grinding stage are presented in Table 1. In general, BC and TC exhibited similar compositions, whereas SW displayed higher SiO_2 and lower Al_2O_3 content compared to the other materials. Comparison of results for each material after each grinding stage revealed minimal changes, except for a significant increase in Fe_2O_3 content in samples ground to a D_{50} of approximately 1 μm due to steel ball wear during high-energy grinding. Regarding composition, Table 4 demonstrates an increase in amorphous phases with decreasing particle size, attributed to structural alterations induced by high-energy grinding [44]. The density values presented in Table 3 correlate with the findings of the oxide and mineralogical composition analyses.

X-ray diffraction patterns, shown in Fig. 2, revealed high crystallinity in BC (Fig. 2a), TC (Fig. 2b), and SW (Fig. 2c) samples and that the 15-μm samples exhibited a subtle difference in composition, including the predominance of quartz. In all samples, a noticeable increase in the intensity of the iron peak was observed with the extension of the grinding times. Analysis of the diffractograms also revealed an increase in the breadth of the peak bases as the particle size decreased, as can be observed in the insets of Fig. 2. This peak

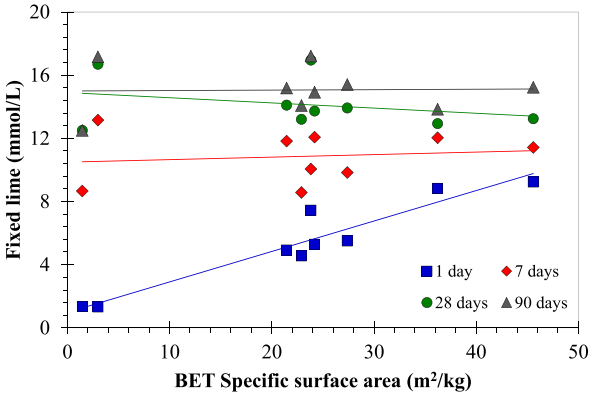

Fig. 4. Relationship between BET specific surface area and fixed lime of BC, TC, and SW samples.

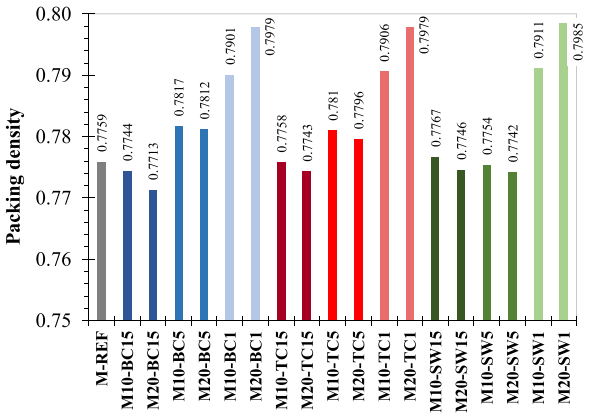

Fig. 5. Values of packing density of reference and mortars containing 10 % and 20 % of BC, TC, and SW.

broadening signifies structural alterations within the crystalline phases induced by the high-energy grinding process, as previously reported by Palaniandy et al. [45].

Through quantitative analysis of these phases (as observed in Table 4), the 1-μm samples exhibited increases by 35.2 %, 36.7 %, and 23.7 % in the amount of amorphous material for brick, tile, and stoneware, respectively, in comparison to the 15-μm samples. Meanwhile, the 5-μm samples did not exhibit a significant change in the amount of amorphous material when compared to the 15-μm samples. Conversely, a reduction in the amount of quartz was observed with the decrease in particle size to 1 μm, suggesting that it represented an important component that underwent amorphization as a result of high-energy milling. Additionally, a reduction was observed in the amount of intermediate microcline and muscovite 2M1, notably in the TC and SW samples, as median particle size reduced from 15 to 1 μm. These minerals belong to the feldspar and phyllosilicate groups and are desirable in suitable quantities in the production of calcined clay products as fluxing agents due to their low melting points. Hence, it can be inferred that grinding modified the crystalline structure of these minerals, contributing to the increase in the amounts of amorphous compounds.

From the pozzolanic point of view, Fig. 3 shows the amount of lime fixed by the different ground materials over time after 1, 7, 28, and 90 days. The results indicated that reducing particle size led to an increase in the amount of fixed lime at 1 and 7 days of testing. However, no such increase was observed in the amount of fixed lime with the reduction in particle size after 28 days, indicating that the pozzolanic reactions predominantly occurred during the first 28 days. Similar results were reported by Hoppe Filho et al. [22]. Changes exceeding 10 % in reactivity due to reduction in particle size from 15 to 5 μm for BC and TC were not observed (Fig. 3a and b). Nonetheless, the reduction in size from 15 to 5 μm for SW resulted in a significant increase in reactivity across all ages studied, as depicted in Fig. 3c. Fig. 4 shows that the fixed lime reactivity at the shortest period studied (1 day) varied significantly with the specific surface area of the samples, irrespective of material. This is a consequence of the greater solubility of the sample phases in alkaline environment with the increase in material specific surface area [46,47]. However, from Fig. 4 it is also possible to observe that such effect does not appear at the longer times studied, since there was no significant variation in fixed lime after, regardless of the type of material evaluated. Yet, the reactivity values found for BC1 (22 %), TC1 (26 %), and SW1 (29 %) were actually higher than those for recognized pozzolans, such as fly ash [48].

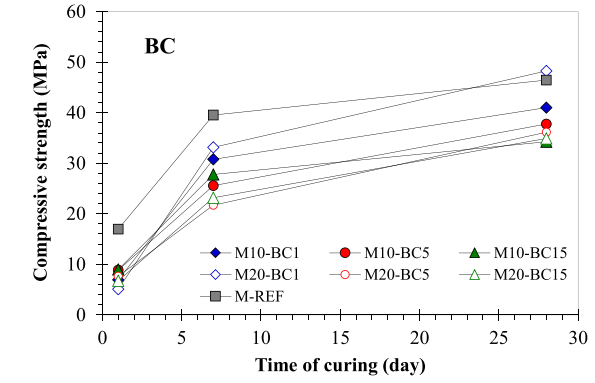

(a)

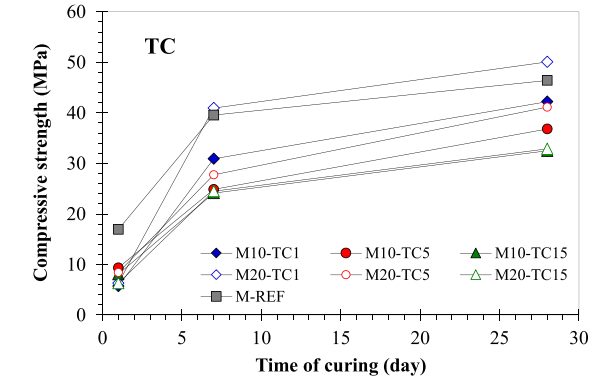

(b)

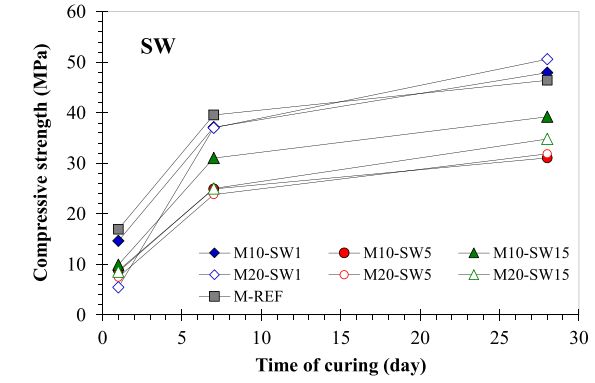

(c)

Fig. 6. Compressive strength values as a function of curing time of reference and mortars with BC (a), TC (b), and SW (c).

3.2. Characterization of cement-based mortars

Fig. 5 shows that the packing density of mortars containing BC and TC increased monotonically with the reduction in particle size compared to the reference mix. For SW-mortars, however, the packing density increase was only observed when D_{50} was reduced to 1 μm. Overall, there was no variation in packing density as a function of cement replacement content by the ground ceramic powders, except for the mixes with 1-μm samples. Thus, the evaluation of packing density using the Compressible Packing Model (CPM) [39] revealed that a significant increase in mortar packing (filling effect) required reducing the particles to D_{50} values below 5 μm. In this aspect, it is worth noting that CPM considered not only the particle size, intentionally kept similar for the tested materials, but also the shape and texture of the particles.

Fig. 6 illustrates the variation in compressive strength of the mortars over curing time. After 1 day of curing, M-BC (Fig. 6a), M-TC

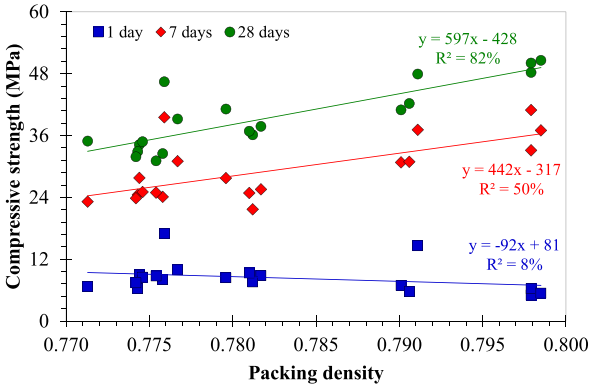

Fig. 7. Relationship between compressive strength and packing density of all mortars.

(Fig. 6b), and M-SW (Fig. 6c) mixes exhibited significantly lower strength values compared to the M-REF, except for M10-SW1. After 7 days of curing, the same behavior was observed; however, at this age, the mixes with SW1 replacement showed no significant differences between each other or with the reference. In the early ages, a pronounced dilution effect was observed for all mortars with ceramic powders, which was partially compensated by the packing density and pozzolanic activity effects, especially for mortars with 1-μm materials. The slower strength gain between 1 and 7 days for M20-SW1 compared to M10-SW1 may be attributed to the higher dosage of superplasticizer used in the mortar with 20 % SW1 (three times higher than in M10-SW1), as shown in Table 2. At 7 days, it is also important to highlight the high strength of M20-TC1, which showed no significant differences compared to the M-REF and the two mixes with SW1. In this case, the high packing density (Fig. 5) of M20-TC1 and the high fixed lime reached at 7 days by TC1 when compared to the other TC samples should be highlighted.

At 28 days, the superior performance of mortars with finer materials was notable and occurred for all three types of ceramics. At this age, M20-BC1 and M10-BC1 showed no significant differences compared to the M-REF and were more resistant than all mortars with BC5 and BC15. For mortars with TC, only M20-TC1 showed no significant difference in compressive strength compared to the reference. The two mixes with SW1 showed statistically equivalent strengths in comparison to M-REF. In this case, M10-SW1 exhibited significantly higher strength than M20-SW1. Fig. 7 shows the influence of packing density on compressive strength and confirms the importance of reducing the particle sizes of the three ceramic powders to increase the compressive strength of mortars when replacing cement replacement in levels of 10 and 20 %. Furthermore, the approximately constant compressive strength values in relation to packing density at 1 day indicate that the strength gains were more influenced by the increased pozzolanic activity resulting from the particle size reduction. It is important to note that the high dosages of superplasticizer (Table 2) were likely detrimental to the initial development of strength at 1 day of curing, especially for mixes with the most finely ground materials, which had also the addition of the grinding aid. This effect has been previously observed in mortars with metakaolin [49].

3.3. *Relationship between compressive strength and fixed lime*

The relationship between the values of fixed lime and compressive strength of mortars with BC (Fig. 8a), TC (Fig. 8b), and SW (Fig. 8c) at different curing times appeared reasonably linear. A recent study has also demonstrated a strong correlation between the reactivity test of calcined kaolinitic clays and the compressive strength of blends in standard mortars [50]. In Fig. 8, it can be observed that the curves for powders with a D_{50} of 15 μm and 5 μm were similar, but differed from those with a D_{50} of 1 μm, which showed a more significant increase in compressive strength for a given reactivity. The behavior observed for the 1-μm ceramic powder indicated that the increase in compressive strength exceeded the reactivity of these particles over time. The SW curves with particle sizes of 15 μm and 5 μm exhibited differences due to the reduced compressive strength of mortars with a particle size of 5 μm. For SW1, the relationship between fixed lime and compressive strength over time was not linear, indicating a physical effect of the particles contributing to a greater increase in compressive strength compared to BC1 and TC1. No clear effects were observed for the different levels of cement replacement studied.

Given the relatively complex relationships of compressive strength and packing density (Fig. 7) and fixed lime (Fig. 8) for the different materials, an attempt was made to represent the compressive strengths at all ages using multiple linear regression using the software Minitab 17. The independent variables studied were packing density (Packing), percent replacement content (Replacement), material type (Type - 1 for TC, 2 for BC, and 3 for SW), percentage of fixed lime (Fixed), percentage of amorphous phases (Amorphous) and D_{50} of the material (Size), given in microns. Curing time and specific surface area were omitted from the model, given their high collinearity with other independent variables. A total of 191 data points were used in the regression, and a stepwise regression, through which individual terms that had p-values larger than 0.05 were removed one-by-one, resulted in a coefficient of determination (R^2) of 0.914 and an adjusted coefficient of determination (R^2_{adj}) of 0.906 for the regression, which was considered satisfactory. Indeed, a comparison between the measured and fitted values is presented in Fig. 9, which shows the reasonably good agreement between the two. The average absolute deviations from measurements and fitted values was 3.3 MPa.

A summary of the results, including values of coefficients (λ values in Equation (1)) and standard errors (SE), is presented in Table 5.

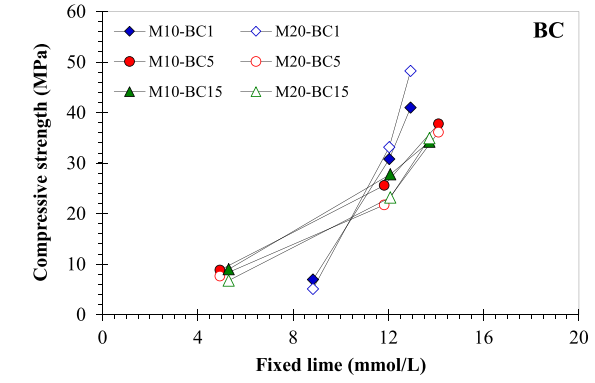

(a)

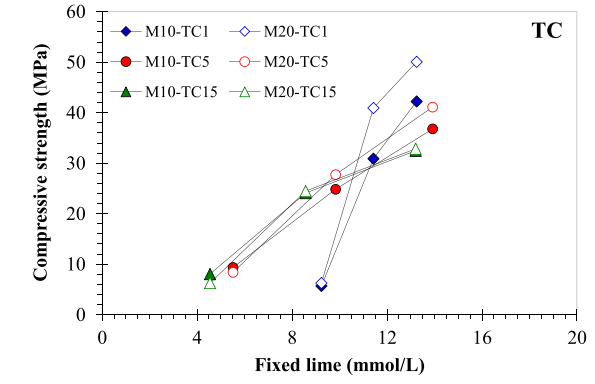

(b)

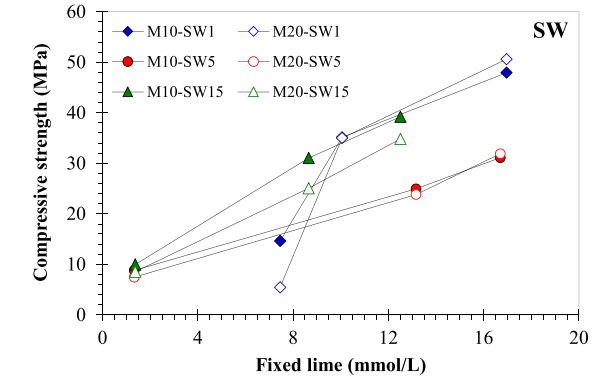

(c)

Fig. 8. Relationship between compressive strength and fixed lime of mortars with BC (a), TC (b), and SW (c).

The main effects of fixed lime, packing density, and type of material were found to influence the compressive strength both linearly and quadratically, whereas the percentage of amorphous material had only a linear relationship with compressive strength. The percentage replacement and the fineness of the materials influenced the compressive strength only through interaction with other variables.

Pore size distribution curves for 20 % BC and SW mortars with the finest and coarsest ground products are shown in Fig. 10. The two mixes containing the coarsest ceramic powders (M20-BC15 and M20-SW15) did not exhibit significant differences in porosity compared to M-REF. This was consistent with the packing density results (Fig. 5) and indicated that no pore refinement occurred when the 15-μm samples were employed. This observation is further supported by the evaluation of the mean diameter of connected pores and threshold diameter values, as presented in Table 6, which showed no significant differences for the M-REF, M20-BC15, and M20-SW15 mixes. Conversely, the reduction in the mean diameter of connected pores relative to M-REF was 47 % and 35 % for M20-BC1

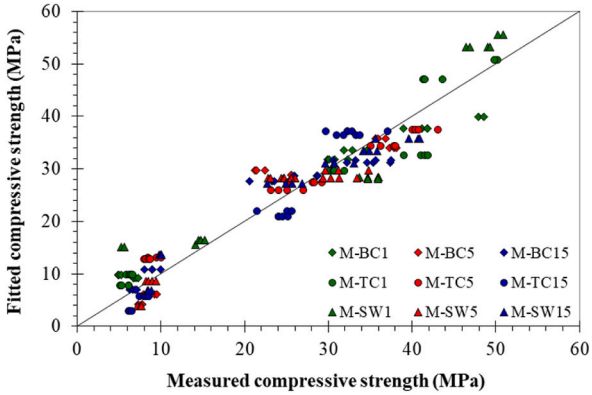

Fig. 9. Comparison of fitted and measured compressive strengths for mortars with the different ceramic materials.

Table 5
Summary of multiple linear regression results of compressive strength of the mortars (terms found to be statistically significant at a value of α equal to 0.05).

Term	Coefficient (λ)	SE coefficient	p-value
Constant	−46656	12435	<0.001
Fixed	331.8	44.7	<0.001
Material	−1069	114	<0.001
Packing	120243	31900	<0.001
Amorphous	−6.288	0.53	<0.001
Fixed*Fixed	−0.1077	0.0248	<0.001
Material*Material	5.666	0.677	<0.001
Packing*Packing	−77110	20470	<0.001
Fixed*Packing	−452.3	59.6	<0.001
Fixed*Amorphous	0.7875	0.0611	<0.001
Fixed*Replacement	0.0398	0.0106	<0.001
Fixed*Size	−0.2301	0.0308	<0.001
Material*Packing	1340	145	<0.001
Material*Replacement	−0.1388	0.0578	0.017
Material*Size	0.8597	0.0956	<0.001
Replacement*Size	−0.02083	0.00912	0.024

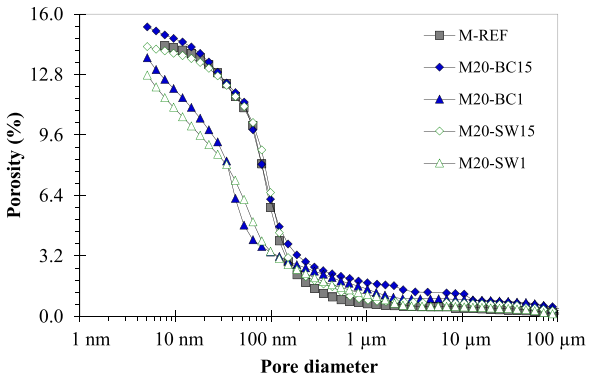

Fig. 10. Total porosity over pore diameter measured by mercury intrusion porosimetry for M-REF and mortars with 20 % of BC1, BC15, SW1, and SW15.

and M20-SW1, respectively. Additionally, M20-SW1 exhibited a 19 % reduction in threshold diameter compared to M-REF, while the reduction for M20-BC1 was even greater, reaching 57 % in comparison to M-REF. Consequently, it was observed that the addition of 1-μm particles led to a reduction in mortar pore sizes. This densification of the porous structure in both M20-BC1 and M20-SW1 was consistent with their higher packing density values, presented in Fig. 5. The densification effect on the pore structure in mortar was previously noted with a 20 % cement replacement by ultrafine ceramic powder [51].

Table 6
Pore parameters from mercury intrusion porosimetry for M-REF and BC and SW mixes.

Mortar	Porosity (%)	Diameter of the connected pores (nm)	Threshold diameter (nm)
M-REF	14.5	79.6	186.0
M20-BC15	15.3	79.6	150.4
M20-BC5	16.5	64.4	121.6
M20-BC1	13.7	42.2	79.5
M20-SW15	14.3	98.4	186.0
M20-SW5	14.4	42.2	121.5
M20-SW1	12.8	52.1	150.4

4. Conclusions

Based on the results presented, it can be concluded that:

- Ceramic tile presented significantly higher grindability, that is, demanded significantly less energy to reach the same level of fineness than ceramic brick and stoneware, demonstrating that if they are ground together as part of demolition waste, fragments of ceramic tile will be finer than those of the other materials.
- The reduction in particle size did not change significantly the oxide composition of the materials by contamination, with XRD analyses showing that high-energy grinding changed marginally the structure of the materials. However, high-energy grinding with steel balls was responsible for significant contamination of the ceramic powders with iron, in particular for the samples ground to the finest size (D_{50} of 1 μm).
- Lime fixation by the samples occurred significantly up to 28 days of testing. However, the effect of particle size (and specific surface area) on reactivity was significant only in the 1-day evaluation.
- Reduction in particle sizes by grinding promoted an improvement in compressive strength, being more significant in mortars containing stoneware ground to the finest size studied (1 μm). The increase in strength was greater than the reactivity of these particles over curing time due to the physical effect of the 1-μm particles. From multiple linear regression analyzes, it was found that compressive strength increased with the increase in the amount of fixed lime, packing density and type of ceramic powder, exhibiting an additional quadratic effect for the first two, besides several synergic effects.
- The effect of reducing particle size on mechanical properties has also found to be associated to reduction in porosity. Indeed, reduction in pore size threshold was associated to the packing density and pozzolanic effects of ceramic materials.

Future research should explore several areas to further understand and enhance the use of ceramic waste in construction materials. Firstly, studies should investigate the optimization of grinding processes to minimize contamination while maximizing the pozzolanic activity and physical effects of ceramic powders. Additionally, the long-term durability performance of concrete and mortar containing finely ground ceramic waste need to be evaluated under various environmental conditions. Finally, the economic feasibility and environmental impact of large-scale implementation of ceramic waste as SCM should be assessed to support its adoption in the cement industry.

CRediT authorship contribution statement

Luciane Farias Ribas: Writing – review & editing, Writing – original draft, Methodology, Investigation, Formal analysis, Data curation. **Guilherme Chagas Cordeiro:** Writing – review & editing, Writing – original draft, Visualization, Formal analysis. **Romildo Dias Toledo Filho:** Writing – review & editing, Writing – original draft, Supervision, Project administration, Funding acquisition, Conceptualization. **Moises Frías:** Writing – review & editing, Resources, Investigation. **Luis Marcelo Tavares:** Writing – review & editing, Writing – original draft, Supervision, Software, Methodology, Investigation, Formal analysis, Conceptualization.

Data availability statement

The datasets generated and/or analyzed during the current study will be available from the corresponding author on reasonable request.

Ethical statement

This manuscript does not involve any ethical issues.

Additional information

No additional information is available for this paper.

Declaration of competing interest

The authors declare that they have no known competing financial interests or personal relationships that could have appeared to influence the work reported in this paper.

Acknowledgements

This study was financed in part by the Coordenação de Aperfeiçoamento de Pessoal de Nível Superior - Brasil (CAPES) - Finance Code 001. The authors would like to thank the support from NUCAT-COPPE-UFRJ and CETEM in FRX and X-ray diffraction analyzes. The financial support from the Brazilian agencies CNPq, FAPERJ, and FAPEAM is also deeply acknowledged. Special thanks for support on the saturated lime dissolution test at the CRM Department in Madrid, Spain.

References

[1] R. Jin, B. Li, T. Zhou, D. Wanatowski, P. Piroozfar, An empirical study of perceptions towards construction and demolition waste recycling and reuse in China, Resour. Conserv. Recycl. 126 (2017) 86–98, https://doi.org/10.1016/j.resconrec.2017.07.034.
[2] Z. He, A. Shen, H. Wu, W. Wang, L. Wang, C. Yao, J. Wu, Research progress on recycled clay brick waste as an alternative to cement for sustainable construction materials, Construct. Build. Mater. 274 (2021) 122113, https://doi.org/10.1016/j.conbuildmat.2020.122113.
[3] M. Bravo, J. de Brito, L. Evangelista, J. Pacheco, Durability and shrinkage of concrete with CDW as recycled aggregates: benefits from superplasticizer's incorporation and influence of CDW composition, Construct. Build. Mater. 168 (2018) 818–830, https://doi.org/10.1016/j.conbuildmat.2018.02.176.
[4] U. Chandru, A. Bahurudeen, R. Senthilkumar, Systematic comparison of different recycled fine aggregates from construction and demolition wastes in OPC concrete and PPC concrete, J. Build. Eng. 75 (2023) 106768, https://doi.org/10.1016/j.jobe.2023.106768.
[5] I.A. Beja, R. Motta, L.B. Bernucci, Application of recycled aggregates from construction and demolition waste with Portland cement and hydrated lime as pavement subbase in Brazil, Construct. Build. Mater. 258 (2020) 119520, https://doi.org/10.1016/j.conbuildmat.2020.119520.
[6] H. Wu, Q. Yong, J. Wang, W. Lu, Z. Qiu, R. Chen, B. Yu, Developing a regional scale construction and demolition waste landfill landslide risk rapid assessment approach, Waste Manag. Res. 184 (2024) 109–119, https://doi.org/10.1016/j.wasman.2024.05.042.
[7] J.L. Li, X. Shen, J. Liu, W. Li, C. Zhong, X. Zhou, The feasibility analysis of recycled aggregates from construction and demolition waste for permeable pavement, KSCE J. Civ. Eng. 27 (2023) 535–550, https://doi.org/10.1007/s12205-022-0767-0.
[8] S. Islam, J. Islam, N.M.R. Hoque, Improvement of consolidation properties of clay soil using fine-grained construction and demolition waste, Heliyon 8 (2022) E11029, https://doi.org/10.1016/j.heliyon.2022.e11029.
[9] D.Y. Ouédraogo, A. Lafitte, R. Sordello, F. Pozzi, I. Mikajlo, J.H.R. Araujo, Y. Reyjol, T.Z. Lerch, Existing evidence on the potential of soils constructed from mineral wastes to support biodiversity: a systematic map, Environ. Evid. 13 (2024) 9, https://doi.org/10.1186/s13750-024-00332-7.
[10] D. Gaudrel, A. Phelipot-Mardelé, C. Lanos, Supersulfated cement formulation using recycled gypsum from building waste, in: C. Ha-Minh, et al. (Eds.), Proceedings of the 7th International Conference on Geotechnics, Civil Engineering and Structures, CIGOS 2024, 4-5 April, Ho Chi Minh City, Vietnam. CIGOS 2024. Lecture Notes in Civil Engineering, vol. 482, Springer, Singapore, 2024, https://doi.org/10.1007/978-981-97-1972-3_73.
[11] R. Mills, Holbein Gardens: delivering a low-carbon structure with reclaimed steel, Struct. Eng. 101 (3) (2023) 30–36, https://doi.org/10.56330/CRPP8446.
[12] P. Ghisellini, M. Ripa, S. Ulgiati, Exploring environmental and economic costs and benefits of a circular economy approach to the construction and demolition sector. A literature review, J. Clean. Prod. 178 (2018) 618–643, https://doi.org/10.1016/j.jclepro.2017.11.207.
[13] D. Caro, C. Lodato, A. Damgaard, J. Cristóbal, G. Foster, F. Flachenecker, D. Tonini, Environmental and socio-economic effects of construction and demolition waste recycling in the European Union, Sci. Total Environ. 908 (2024) 168295, https://doi.org/10.1016/j.scitotenv.2023.168295.
[14] M. Frías, S. Martínez, R. Vigil, L. Fernández, R. García, Reactivity in cement pastes bearing fine fraction concrete and glass from construction and demolition waste: microstructural analysis of viability, Cem. Concr. Res. 148 (2021) 106531, https://doi.org/10.1016/j.cemconres.2021.106531.
[15] J. Moreno-Juez, Iñigo J. Vegas, M. Frías Rojas, R. Vigil de la Villa, E. Guede-Vázquez, Laboratory-scale study and semi-industrial validation of viability of inorganic CDW fine fractions as SCMs in blended cements, Construct. Build. Mater. 271 (2021) 121823, https://doi.org/10.1016/j.conbuildmat.2020.121823.
[16] Z. Prošek, V. Nežerka, R. Hlůžek, J. Trejbal, P. Tesárek, G. Karra'a, Role of lime, fly ash, and slag in cement pastes containing recycled concrete fines, Construct. Build. Mater. 201 (2019) 702–714, https://doi.org/10.1016/j.conbuildmat.2018.12.227.
[17] Z. Li, Y. Bian, J. Zhao, Y. Wang, Z. Yuan, Recycled concrete fine powder (RFP) as cement partial replacement: influences on the physical properties, hydration characteristics, and microstructure of blended cement, J. Build. Eng. 62 (2022) 105326, https://doi.org/10.1016/j.jobe.2022.105326.
[18] X. Deng, H. Guo, H. Tan, X. He, Z. Zheng, Y. Su, J. Yang, An accelerator prepared from waste concrete recycled powder and its effect on hydration of cement-based materials, Construct. Build. Mater. 296 (2021) 123767, https://doi.org/10.1016/j.conbuildmat.2021.123767.
[19] A.M. Pitarch, L. Reig, A.E. Tomás, G. Forcada, L. Soriano, M.V. Borrachero, J. Payá, J.M. Monzó, Pozzolanic activity of tiles, bricks and ceramic sanitary-ware in eco-friendly Portland blended cements, J. Clean. Prod. 279 (2021) 123713, https://doi.org/10.1016/j.jclepro.2020.123713.
[20] L. Reig, et al., Ceramic waste: reuse as a recycled aggregate, in: D. Bienvenido-Huertas, J. Durán-Álvarez (Eds.), Building Engineering Facing the Challenges of the 21st Century. Lecture Notes in Civil Engineering, vol. 345, Springer, Singapore, 2023, https://doi.org/10.1007/978-981-99-2714-2_29.
[21] J. Shao, J. Gao, Y. Zhao, X. Chen, Study on the pozzolanic reaction of clay brick powder in blended cement pastes, Construct. Build. Mater. 213 (2019) 209–215, https://doi.org/10.1016/j.conbuildmat.2019.03.307.
[22] J. Hoppe Filho, C.A.O. Pires, O.D. Leite, M.R. Garcez, M.H.F. Medeiros, Red ceramic waste as supplementary cementitious material: microstructure and mechanical properties, Construct. Build. Mater. 296 (2021) 123653, https://doi.org/10.1016/j.conbuildmat.2021.123653.
[23] E.M.J. Berodier, K.L. Scrivener, Understanding the filler effect on the nucleation and growth of C-S-H, J. Am. Ceram. Soc. 97 (12) 3764-3773. http://doi.wiley.com/10.1111/jace.13177.
[24] Y. Zhao, J. Gao, C. Liu, X. Chen, Z. Xu, The particle-size effect of waste clay brick powder on its pozzolanic activity and properties of blended cement, J. Cleaner Prod. 242 (2020) 118521, https://doi.org/10.1016/j.jclepro.2019.118521.
[25] S. Li, G. Chen, Z. Xu, X. Luo, J. Gao, Particle-size effect of recycled clay brick powder on the pore structure of blended cement paste, Construct. Build. Mater. 344 (2022) 128288, https://doi.org/10.1016/j.conbuildmat.2022.128288.
[26] P.R. de Matos, R.D. Sakata, L. Onghero, V.G. Uliano, J. de Brito, C.E.M. Campos, P.J.P. Gleize, Utilization of ceramic tile demolition waste as supplementary cementitious material: an early-age investigation, J. Build. Eng. 38 (2021) 102187, https://doi.org/10.1016/j.jobe.2021.102187.
[27] L. Li, W. Liu, Q. You, M. Chen, Q. Zeng, Waste ceramic powder as a pozzolanic supplementary filler of cement for developing sustainable building materials, J. Clean. Prod. 259 (2020) 120853, https://doi.org/10.1016/j.jclepro.2020.120853.
[28] S.E. Schulze, J. Rickert, Suitability of natural calcined clays as supplementary cementitious material, Cem. Concr. Compos. 95 (2019) 92–97, https://doi.org/10.1016/j.cemconcomp.2018.07.006.
[29] A.A. de Siqueira, G.C. Cordeiro, Properties of binary and ternary mixes of cement, sugarcane bagasse ash and limestone, Construct. Build. Mater. 317 (2022) 126150, https://doi.org/10.1016/j.conbuildmat.2021.126150.
[30] ABNT NBR 7214, Standard sand for cement tests - specification. Brazilian Association of Technical Standards, 2015.
[31] G.C. Cordeiro, P.V. Andreão, L.M. Tavares, Pozzolanic properties of ultrafine sugar cane bagasse ash produced by controlled burning, Heliyon 5 (2019) e02566, https://doi.org/10.1016/j.heliyon.2019.e02566.

[32] F.C. Bond, Third theory of comminution, T. Soc. Min. Eng. 153 (1952) 484–494.
[33] ABNT NBR NM 18, Portland Cement - Chemical Analysis - Determination of Loss on Ignition, Brazilian Association of Technical Standards, 2012.
[34] M. Frias, M.I.S. de Rojas, J. Cabrera, The effect that the pozzolanic reaction of metakaolin has on the heat evolution in metakaolin-cement mortars, Cem. Concr. Res. 30 (2000) 209–216, https://doi.org/10.1016/S0008-8846(99)00231-8.
[35] ABNT NBR 7215, Portland cement - determination of compressive strength of cylindrical test specimens. Brazilian Association of Technical Standards, 2019.
[36] I. International Organization for Standardization, ISO 15901-1: evaluation of pore size distribution and porosimetry of solid materials by mercury porosimetry and gas adsorption - Part 1: mercury porosimetry, Switzerland, https://www.iso.org/standard/56005.html, 2016. (Accessed 6 October 2020).
[37] R.A. Cook, K.C. Hover, Experiments on the contact angle between mercury and hardened cement paste, Cem. Concr. Res. 21 (6) (1991) 1165–1175, https://doi.org/10.1016/0008-8846(91)90077-U.
[38] D.C. Montgomery, G.C. Runger, Applied Statistics and Probability for Engineers, John Wiley & Sons, 2011.
[39] F. De Larrard, Concrete Mixture Proportioning, CRC Press, 1999, https://doi.org/10.1201/9781482272055.
[40] T. Sedran, F. de Larrard, RENÉ-LCPC – Un logicel pour optimiser la granularité des matériaux de génie civil, Technical Note, Bulletin de Liaison des Laboratoires des Ponts et Chaussées, 1994.
[41] L.M. Tavares, R.D.C. Kallemback, Grindability of binary ore blends in ball mills, Miner. Eng. 41 (2013) 115–120, https://doi.org/10.1016/j.mineng.2012.11.001.
[42] L. Ribas, G.C. Cordeiro, R.D. Toledo Filho, L.M. Tavares, Measuring the strength of irregularly-shaped fine particles in a microcompression tester, Miner. Eng. 65 (2014) 149–155, https://doi.org/10.1016/j.mineng.2014.05.021.
[43] K.P. Alvarenga, G.C. Cordeiro, Evaluating sugarcane bagasse fly ash as a sustainable cement replacement for enhanced performance, Clean. Eng. Technol. 20 (2024) 100751, https://doi.org/10.1016/j.clet.2024.100751.
[44] Y. Li, J. Fang, L. Cheng, X. He, Y. Su, H. Tan, Mechanical performance, hydration characteristics and microstructures of high volume blast furnace ferronickel slag cement mortar by wet grinding activation, Construct. Build. Mater. 320 (2022) 126148, https://doi.org/10.1016/j.conbuildmat.2021.126148.
[45] S. Palaniandy, K.A.M. Azizli, H. Hussin, S.F.S. Hashim, Study on mechanochemical effect of silica for short grinding period, Int. J. Miner. Process. 82 (2007) 195–202, https://doi.org/10.1016/j.minpro.2006.10.008.
[46] G.C. Cordeiro, K.E. Kurtis, Effect of mechanical processing on sugar cane bagasse ash pozzolanicity, Cem. Concr. Res. 97 (2017) 41–49, https://doi.org/10.1016/j.cemconres.2017.03.008.
[47] A.A. Mota dos Santos, G.C. Cordeiro, Investigation of particle characteristics and enhancing the pozzolanic activity of diatomite by grinding, Mater. Chem. Phys. 270 (2021) 124799, https://doi.org/10.1016/j.matchemphys.2021.124799.
[48] M.I. Sánchez de Rojas, F. Marín, J. Rivera, M. Frías, Morphology and properties in blended cements with ceramic wastes as a pozzolanic material, J. Am. Ceram. Soc. 89 (2006) 3701–3705, https://doi.org/10.1111/j.1551-2916.2006.01279.x.
[49] M. Sonebi, M. Lachemi, K.M.A. Hossain, Optimisation of rheological parameters and mechanical properties of superplasticised cement grouts containing metakaolin and viscosity modifying admixture, Construct. Build. Mater. 38 (2013) 126–138, https://doi.org/10.1016/j.conbuildmat.2012.07.102.
[50] F. Avet, R. Snellings, A. Alujas Diaz, M. Ben Haha, K. Scrivener, Development of a new rapid, relevant and reliable (R^3) test method to evaluate the pozzolanic reactivity of calcined kaolinitic clays, Cem. Concr. Res. 85 (2016) 1–11, https://doi.org/10.1016/j.cemconres.2016.02.015.
[51] L.G. Li, Z.Y. Zhuo, J. Zhu, J.J. Chen, A.K.H. Kwan, Reutilizing ceramic polishing waste as powder filler in mortar to reduce cement content by 33% and increase strength by 85, Powder Technol. 355 (2019) 119–126, https://doi.org/10.1016/j.powtec.2019.07.043.